Inorganic Chemistry

Article

pubs.acs.org/IC

Oxo-Exchange of Gas-Phase Uranyl, Neptunyl, and Plutonyl with Water and Methanol

Ana F. Lucena,[†,△] Samuel O. Odoh,[‡,∥,△] Jing Zhao,[§] Joaquim Marçalo,[†] Georg Schreckenbach,*[,∥] and John K. Gibson*[,⊥]

[†]Centro de Ciências e Tecnologias Nucleares, Instituto Superior Técnico, Universidade de Lisboa, 2695-066 Bobadela LRS, Portugal

[‡]Environmental and Molecular Science Laboratory, Pacific Northwest National Laboratory, Richland, Washington 99352, United States

[∥]Department of Chemistry, University of Manitoba, Winnipeg, Manitoba, Canada R3T 2N2

[§]Beijing Center for Crystal Research and Development, Key Laboratory of Functional Crystals and Laser Technology, Technical Institute of Physics and Chemistry, Chinese Academy of Sciences, Beijing 100190, China

[⊥]Chemical Sciences Division, Lawrence Berkeley National Laboratory, Berkeley, California 94720, United States

Supporting Information

ABSTRACT: A challenge in actinide chemistry is activation of the strong bonds in the actinyl ions, AnO_2^+ and AnO_2^{2+}, where An = U, Np, or Pu. Actinyl activation in oxo-exchange with water in solution is well established, but the exchange mechanisms are unknown. Gas-phase actinyl oxo-exchange is a means to probe these processes in detail for simple systems, which are amenable to computational modeling. Gas-phase exchange reactions of UO_2^+, NpO_2^+, PuO_2^+, and UO_2^{2+} with water and methanol were studied by experiment and density functional theory (DFT); reported for the first time are experimental results for UO_2^{2+} and for methanol exchange, as well as exchange rate constants. Key findings are faster exchange of UO_2^{2+} versus UO_2^+ and faster exchange with methanol versus water; faster exchange of UO_2^+ versus PuO_2^+ was quantified. Computed potential energy profiles (PEPs) are in accord with the observed kinetics, validating the utility of DFT to model these exchange processes. The seemingly enigmatic result of faster exchange for uranyl, which has the strongest oxo-bonds, may reflect reduced covalency in uranyl as compared with plutonyl.

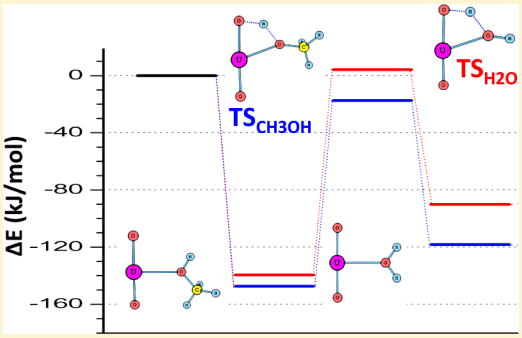

INTRODUCTION

The actinyl ions, AnO_2^+ and AnO_2^{2+}, are important solution species for An = U, Np, and Pu, with UO_2^{2+} being a particularly prevalent species in the chemistry of uranium.[1] The An-O_{yl} bonds in these actinyls are strong, with bond dissociation energies, $D[OAn^{2+}\text{-}O]$, ranging from 403 kJ/mol for PuO_2^{2+} to 529 kJ/mol for UO_2^{2+}; the $D[OAn^{+}\text{-}O]$ bond energies are even greater.[2] Activation of the strong actinyl bonds is a challenge in synthetic actinide chemistry, with a particular focus on functionalization or cleavage of the U−O_{yl} bond in the UO_2^{2+} moiety,[3,4] such as has been accomplished in the conversion of UO_2^{2+} to UO(O-*tert*-butyl)$_4$,[5] and the coordination of the O_{yl} by highly electrophilic Li.[6]

A special case of O_{yl} activation is oxo-exchange with an O-atom donor, principally with water as in eq 1.

$$[AnO_2]^{+/2+} + H_2O^* \rightarrow [AnOO^*]^{+/2+} + H_2O \qquad (1)$$

In eq 1 there is no net change in the chemical composition of the actinyl moiety, but the exchange of O-atoms necessarily proceeds through a mechanism that disrupts the initial $[OAn{=}O]^{+/2+}$ moiety to result in the $[OAn{=}O^*]^{+/2+}$ product. (Note: In eq 1, and throughout this paper, "O" represents the dominant (99.8%) naturally occurring ^{16}O isotope; O* represents ^{17}O or ^{18}O, depending on the experimental method used to study oxo-exchange. The experiments reported here were performed using O-atom donors isotopically enriched in ^{18}O, as specified in the following sections.) The first studies of oxo-exchange by Gordon and Taube in 1961 were performed by reaction between UO_2^{2+} and $H_2{}^{18}O$, followed by precipitation and gravimetric analysis.[7,8] These studies revealed that the rate of oxo-exchange depends on both the H^+ and UO_2^+ concentrations. The proton-dependence suggested a mechanism involving $UO_2(OH)^{2+}$, and the uranyl(V)-dependence indicated that UO_2^+ exchanges more rapidly than UO_2^{2+}. Oxo-exchange in solution can be more directly monitored using isotopic labeling in $H_2{}^{17}O$ and monitoring changes in the ^{17}O NMR spectra.[9,10] The rate of O_{yl}-exchange was determined for UO_2^{2+} by Rabideau under acidic conditions using ^{17}O NMR,[11] with the results in accord with those of Gordon and Taube. These studies revealed that the half-life for uranyl(VI) oxo-exchange under acidic conditions was on the order of ca. 10^4

Received: November 11, 2013
Published: January 31, 2014

   dx.doi.org/10.1021/ic402824k | Inorg. Chem. 2014, 53, 2163−2170

hours, in accord with strong U−O bonds resistant to disruption. Clark et al. studied uranyl(VI) oxo-exchange under highly alkaline conditions and determined an exchange rate of 45 s^{-1},[12] which is several orders of magnitude faster than under acidic conditions and supports the role of hydroxides as key species for enabling facile exchange. Although a rate for direct comparison with uranyl(VI) was not obtained, Clark et al. demonstrated that neptunyl(VI) oxo-exchange was adequately fast that it was complete within two hours;[13] this is much faster than determined by Rabideau for neptunyl(VI) and plutonyl(VI) under acidic conditions.[14,15] Exchange studies for the pentavalent AnO_2^+ ions have revealed that the exchange rate of UO_2^+ is significantly faster than the exchange rates for NpO_2^+ and PuO_2^+,[7,14,15] a result in apparent discord with the stronger bonds in uranyl.

In recent years, a number of theoretical studies have attempted to explain the observed exchange behavior of uranyl,[16−26] most of which invoke monomeric or polymeric hydroxide species comprising one or more uranyl moieties. Although several of these theoretical evaluations are substantiated by experimental observations, such as, for example, ^{17}O NMR magnetization transfer,[20] there is no detailed experimental information to directly confirm any of the proposed mechanisms. Given that it is not yet practical to reliably deduce molecular scale transformations involved in oxo-exchange in solution, we have undertaken to confront the issue in the rarified environment of the gas phase for bare $AnO_2^{+/2+}$ ions. In an initial report on this topic, the comparative exchange rates of UO_2^+, NpO_2^+, and PuO_2^+ with $H_2{}^{18}O$ in the gas phase were reported and rationalized by computed potential energy profiles.[27] In the present work we extend the experimental measurements to UO_2^{2+}, which can be compared with those for UO_2^+. Also reported here are the first quantitative values for the gas-phase oxo-exchange rate constants. Potential energy profiles (PEPs) computed by DFT are reported for all of the studied oxo-exchange processes. Furthermore, experimental studies of oxo-exchange with $CH_3{}^{18}OH$ were performed for comparison with the results for $H_2{}^{18}O$, and to further assess the reliability of the computational modeling to understand exchange mechanisms and efficiencies.

It had previously been proposed that the seemingly enigmatic more facile oxo-activation in exchange of uranyl(V) versus plutonyl(V) with water was a manifestation of greater covalency upon proceeding across the series of actinyls.[27] Although it is known that the actinyls exhibit substantial covalent bonding,[28−30] there is less consensus as to whether covalency in actinide bonds with ligands increases across the actinide series, particularly as the meaning of "covalency" is not necessarily well-defined.[31−35] The issue of actinide covalency and its variation across the actinyl series is evaluated in this work by bonding analyses of the AnO_2^+ and AnO_2^{2+} species, with consideration as to the significance of the conventional concept of covalency for the particular case of the 5f actinides, as has been discussed by Kaltsoyannis.[35]

EXPERIMENTAL PROCEDURES

The experimental approach has been described previously.[36−38] A brief outline of the general approach is included here—the experimental details are in the Supporting Information. The actinide dioxide monopositive cations, AnO_2^+ where An = U, Np, or Pu, were produced by laser desorption ionization (LDI) of solid alloys of Pt containing a few atom percent of the actinide.[37] There was sufficient oxygen contamination in the alloys that the AnO_2^+ ions were produced by LDI. The UO_2^{2+} reactant ion was prepared by oxidation of U^{2+} produced by LDI, using N_2O pulsed into the ICR cell, as described previously.[36] Bimolecular gas-phase reactions of isotopically labeled $H_2{}^{18}O$ and $CH_3{}^{18}OH$ with actinyl cations were studied by Fourier transform ion cyclotron resonance mass spectrometry. Pseudo first-order reaction kinetics for oxo-exchange were determined by isolating and cooling the oxide ions, and measuring the time-dependence of the decay of reactant ions and in-growth of product ions. For comparative purposes, in addition to absolute rate constants, reaction efficiencies are reported as k/k_{COL}, where k_{COL} is the collisional rate constant derived from the modified variational transition-state/classical trajectory theory developed by Su and Chesnavich.[39]

COMPUTATIONAL DETAILS

The scalar relativistic DFT calculations were performed with the NWChem[40] and ADF software suites.[41] The geometry optimizations, transition state searches, and vibrational frequency analyses were carried out with the NWChem code. In these calculations, we employed the scalar relativistic Stuttgart small-core effective core potential[42−44] for the actinide atoms. The triple-ζ polarized (TZVP) basis sets of Godbout et al. were used for the oxygen and hydrogen atoms.[45] The B3LYP density functional was used in these calculations.[46,47] The combination of these pseudopotential and basis sets with this functional (labeled as B3LYP/TZVP level) has been shown to give accurate predictions of the properties and reaction energies of actinide complexes.[21,48−54] The geometry optimizations were performed without symmetry restrictions and were followed by vibrational frequency analysis to determine the local minima or saddle point natures of the optimized structures. The reported reaction energies were obtained by combining the electronic energies with the zero-point vibrational energy corrections.

The Mulliken charge and the binding energy analyses were carried out with the ADF code. The geometries obtained at the B3LYP/TZVP level were used in these calculations. The scalar zeroth order regular approximation (ZORA)[55,56] was used in conjunction with Slater type orbitals (STOs) of TZ2P quality. The decomposition of the binding energies was carried out with the extended transition state method.[57−59]

The calculations on the open-shell actinyl complexes were carried out with unrestricted wave functions. The ground electronic states of these species were all found to be of high-spin character: U^{5+}, f^1; Np^{6+}, f^1; Np^{5+}, f^2; Pu^{6+}, f^2; and Pu^{5+}, f^3. The correct occupations of the 5f orbitals were obtained by swapping the unpaired electrons between various combinations of occupied and unoccupied orbitals.

RESULTS AND DISCUSSION

Experimental Oxo-Exchange Reaction Kinetics. The studied actinyl oxo-exchange reactions are given by eqs 2−5, where An = U, Np, or Pu.

$$AnO_2^+ + H_2{}^{18}O \rightarrow AnO^{18}O^+ + H_2O \quad (2)$$

$$UO_2^{2+} + H_2{}^{18}O \rightarrow UO^{18}O^{2+} + H_2O \quad (3a)$$

$$UO_2^{2+} + H_2{}^{18}O \rightarrow UO^{18}O^+ + H_2O^+ \quad (3b)$$

$$AnO_2^+ + CH_3{}^{18}OH \rightarrow AnO^{18}O^+ + CH_3OH \quad (4)$$

$$UO_2^{2+} + CH_3{}^{18}OH \rightarrow UO^{18}O^+ + CH_3OH^+ \quad (5)$$

The measured pseudo-first order exchange rate constants, k, and efficiencies relative to the collisional rate constants, k/k_{COL}, are given in Table 1 for oxo-exchange with water and in Table 2 for oxo-exchange with methanol. A representative kinetics plot is shown in Figure 1 for the reaction of UO_2^{2+} with $CH_3{}^{18}OH$, for which the three observed products are $UO^{18}O^+$ (oxo-exchange eq 5; 15%), $UO^{18}OH^+$ ($^{18}OH^-$-transfer; 35%), and

dx.doi.org/10.1021/ic402824k | Inorg. Chem. 2014, 53, 2163−2170

Table 1. Experimental Results for Actinyl Oxo-Exchange with $H_2{}^{18}O$[a]

	k	k_{COL}	k/k_{COL}
UO_2^+/eq 2	0.00046	2.220	0.00021
NpO_2^+/eq 2	<0.00003	2.220	<0.00002
PuO_2^+/eq 2	<0.00003	2.219	<0.00002
UO_2^{2+}/eqs 3a and 3b[b]	0.171	4.439	0.039

[a]Pseudo first-order rate constants, k and k_{COL} in units of 10^{-9} cm^3 molecule^{-1} s^{-1}, and reaction efficiencies, k/k_{COL}, for the oxo-exchange reactions given by eqs 2, 3a, 3b, and 4. [b]The exchange reactions accounted for 55% of the products. The product distribution was: 35% $UO^{18}O^{2+}$ (eq 4a), 20% $UO^{18}O^+$ (eq 4b), and 45% UO_2^+ (electron-transfer to $H_2{}^{18}O$). The reported k and k/k_{COL} are for the exchange reactions only; the total rate constant for exchange and charge-transfer is $k = 0.311 \times 10^{-9}$ cm^3 molecule^{-1} s^{-1}.

Table 2. Experimental Results for Actinyl Oxo-Exchange with $CH_3{}^{18}OH$[a]

	k	k_{COL}	k/k_{COL}
UO_2^+/eq 4	0.00070 (0.00106)[b]	1.694	0.00042 (0.00062)[b]
NpO_2^+/eq 4	<0.00003 (0.00176)[b]	1.695	<0.00002 (0.00104)[b]
PuO_2^+/eq 4	<0.00003 (0.00173)[b]	1.693	<0.00002 (0.00102)[b]
UO_2^{2+}/eq 5[c]	0.203	3.388	0.060

[a]Pseudo first-order rate constants, k and k_{COL} in units of 10^{-9} cm^3 molecule^{-1} s^{-1}, and reaction efficiencies, k/k_{COL}, for the oxo-exchange reactions given by eqs 4 and 5. [b]Inefficient formation of adducts, $AnO_2(CH_3{}^{18}OH)^+$, was observed with k and k/k_{COL} as given in parentheses. [c]The values for k and k/k_{COL} are for oxo-exchange with charge separation according to eq 5, which accounted for only 15% of the products of the reaction of $UO_2^{2+} + CH_3{}^{18}OH$. The other products were $UO_2(^{18}OH)^+$ (35%) and UO_2^+ (50%).

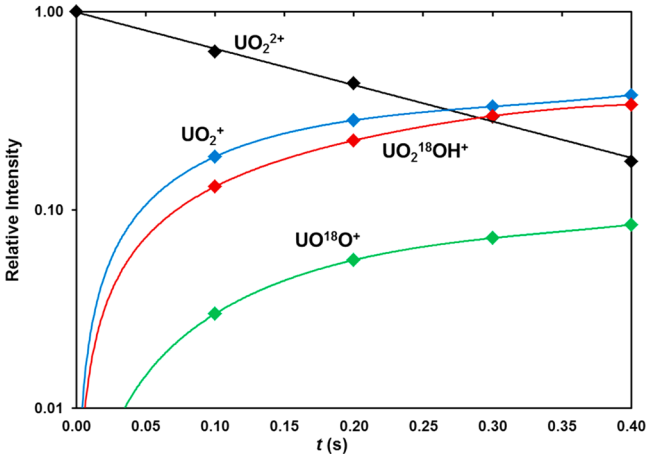

Figure 1. Pseudo-first-order kinetics plot for the reaction of UO_2^{2+} with $CH_3{}^{18}O$. The ingrowth of the three bimolecular reaction products, UO_2^+, $UO_2{}^{18}OH^+$, and $UO^{18}O^+$, results in the overall pseudo-first-order linear decay of the semilogaritmic plot of the decay of UO_2^{2+} vs reaction time that provides a net rate constant $k = 1.350 \times 10^{-9}$ cm^3 molecule^{-1} s^{-1}. The partial rate constant for charge-transfer oxo-exchange to produce $UO^{18}O^+$ is $k = 0.203 \times 10^{-9}$ cm^3 molecule^{-1} s^{-1}.

UO_2^+ (electron-transfer; 50%). Qualitative results previously reported for eq 2 are in accord with the measured rate constants for the AnO^+ given in Table 1.[27] Oxo-exchange was observed for UO_2^+ and UO_2^{2+} with both water and methanol; partial or complete electron-transfer from the neutral ligand to UO_2^{2+} occurred concomitant with oxo-exchange. The NpO_2^+ and PuO_2^+ ions did not exhibit oxo-exchange with either water or methanol to within the experimental detection limit of ~0.002% efficiency. Although hydrates were not observed, all three of the $AnO_2(CH_3{}^{18}OH)$ adducts were produced inefficiently ($k/k_{COL} \approx 0.001$); the appearance of methanol adducts, but not hydrates, is attributed to the greater capability of CH_3OH to dissipate coordination energy as compared with the smaller H_2O ligand.[60] Collision induced dissociation (CID) of the three $AnO_2(CH_3{}^{18}OH)^+$ resulted exclusively in elimination of $CH_3{}^{18}OH$, confirming that oxo-exchange had not occurred in the adducts to produce $AnO^{18}O(CH_3OH)^+$.

The reaction of UO_2^{2+} with $H_2{}^{18}O$ resulted in three products, $UO^{18}O^{2+}$ (+ H_2O; eq 3a; 35%), $UO^{18}O^+$ (+ H_2O^+; eq 3b; 20%), and UO_2^+ (+ $H_2{}^{18}O^+$; 45%). The net oxo-exchange rate constant is given by the sum of those for eqs 3a and 3b. Oxo-exchange of UO_2^{2+} with methanol was exclusively accompanied by electron-transfer from CH_3OH to produce $UO^{18}O^+$ (eq 5). The occurrence of electron-transfer to all of the $UO^{18}O^{2+}$ oxo-exchange product with methanol but to only 20% of the oxo-exchange product with water reflects the higher ionization energy of water: IE[H_2O] = 12.6 eV; IE[CH_3OH] = 10.9 eV.[61] As discussed below, the oxo-exchange kinetics for UO_2^{2+} are determined by processes that occur in the dipositive uranyl species; charge-separation by electron transfer from the neutral O-atom donor occurs after exchange has occurred, during elimination of the water or methanol molecule from the exchange product, and therefore does not affect the observed exchange kinetics. Oxo-exchange of UO_2^+ is inefficient, 0.02% with water and 0.04% with methanol; oxo-exchange of UO_2^{2+} is significantly more efficient, 3.9% with water and 6.0% with methanol. The following key comparisons of oxo-exchange efficiencies (k/k_{COL}) are evident from the results in Tables 1 and 2:

- The oxo-exchange efficiencies of UO_2^+ and UO_2^{2+} with $CH_3{}^{18}O$ are greater than with $H_2{}^{18}O$ by a factor of 1.5–2.
- For both $H_2{}^{18}O$ and $CH_3{}^{18}OH$, the oxo-exchange efficiencies with UO_2^+ are more than 10 times greater than with NpO_2^+ or PuO_2^+.
- For both $H_2{}^{18}O$ and $CH_3{}^{18}OH$, the oxo-exchange efficiencies with UO_2^{2+} are more than 100 times greater than with UO_2^+.

Potential Energy Profiles: Relationships to Observed Oxo-Exchange Kinetics. To understand the underlying basis for the observed k/k_{COL} differences between water and methanol, between the three AnO_2^+ (An = U, Np, Pu), and between UO_2^{2+} and UO_2^+, PEPs were computed for the pertinent exchange reactions, as discussed below.

Water versus Methanol. The calculated PEPs for exchange of UO_2^+ with water and methanol are shown in Figure 2, with the structures of reactants **1**, transition states **3** and **5**, and intermediates **2**, **4**, and **6** shown in Figure 3, and the energetics of reactions involving species **1**–**4** given in Tables 3–5. In the initial reaction, **1**–**2**, the water or methanol ligand is coordinated to uranyl. This is followed by H-atom transfer from the ligand to the uranyl axial group, resulting in the formation of equatorial hydroxo or methoxy ligands (**2**–**4**; Figure 3). The **2**–**4** reaction has the largest transition barrier **3** and is thus presumed to be the rate determining step (Figure 2). Intermediate **4** then undergoes rearrangement reactions that lead to the second intermediate **6**, which has an axial methoxy ligand in the reaction with methanol, and has interchanged the axial and equatorial hydroxo groups in the reaction with water.

dx.doi.org/10.1021/ic402824k | Inorg. Chem. 2014, 53, 2163–2170

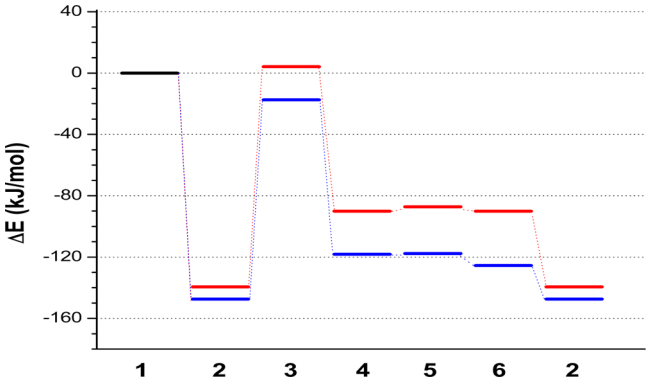

Figure 2. Potential energy profiles for the oxo-exchange reactions of UO_2^+ with water (red) and methanol (blue). The energies are relative to the reactant asymptotes. The PEPs are similar for NpO_2^+ and PuO_2^+ although with substantially different energies. The structures of the species are shown in Figure 3. The energies for **1**−**2** and **2**−**4** are in Tables 3 and 4, respectively. The transition state barrier heights (**3**) of the **2**−**4** reactions, as well as the energy of **3** relative to the reactant asymptote, are provided in Table 5

The rearrangement reactions **4**−**6** generally have very small transition state barriers. The oxo-exchange process is completed by the elimination of H_2O or CH_3OH from the association complex **2** to produce the reactant uranyl ion **1** in which an O atom has been replaced by an ^{18}O atom, $UO^{18}O^+$. As the only difference between the reactants and products is exchange of ^{16}O and ^{18}O atoms, the reactions are essentially thermoneutral.

The efficiency of a reaction under the near-thermal conditions of the experiments should correlate with the energy of the highest energy species along the PEP, which is **3** for the oxo-exchange reactions: the farther below the reactant energies ($E[\mathbf{1}] \equiv 0$) the highest transition state lies, the more facile the reaction should be. The transition state **3** in Figure 2 for the

Table 3. Energies (kJ/mol) Obtained for the Complex Formation Reactions 1−2 in the Gas Phase

	water	methanol	ethanol	*i*-propanol	*t*-butanol
UO_2^+	−139.5	−147.4	−162.9	−166.0	−165.0
NpO_2^+	−139.6	−159.6	−180.3	−187.3	−186.6
PuO_2^+	−139.8	−157.9	−168.5	−175.2	−173.9
UO_2^{2+}	−279.8	−344.0	−381.3		

Table 4. Energies (kJ/mol) Obtained for the Oxo-Protonation (2−4 Reactions) of the Axial Oxo-Atoms by the Acidic Protons of Water and Several Alcohols

	water	methanol	ethanol	propan-2-ol	*t*-butanol
UO_2^+	49.4	29.2	32.9	34.2	30.2
NpO_2^+	73.1	63.6	79.2	81.7	78.2
PuO_2^+	114.5	102.7	114.0	110.8	106.4
UO_2^{2+}	92.7	76.5			

UO_2^+/water reaction lies slightly above the reactant asymptote, at 4.2 kJ/mol (Table 5). This energy is within the computational uncertainty; furthermore, at 300 K the translational energy is ∼4 kJ/mol and the reactants possess additional internal energy that may be available to surmount such minor barriers. It is thus reasonable that this oxo-exchange reaction proceeds albeit very inefficiently (k/k_{COL} = 0.00021). For the UO_2^+/methanol reaction, transition state **3** is ∼22 kJ/mol lower than that for the water reaction and 17.5 kJ/mol below the reactants **1** (Figure 2, Table 5). It is thus predicted that oxo-exchange of UO_2^+ with methanol should occur more efficiently than with water. The experimental result is that exchange with methanol occurs twice as efficiently as with water (Tables 1 and 2).

The conversion of the association complexes **2** to intermediates **4** results from cleaving an O−H bond in water

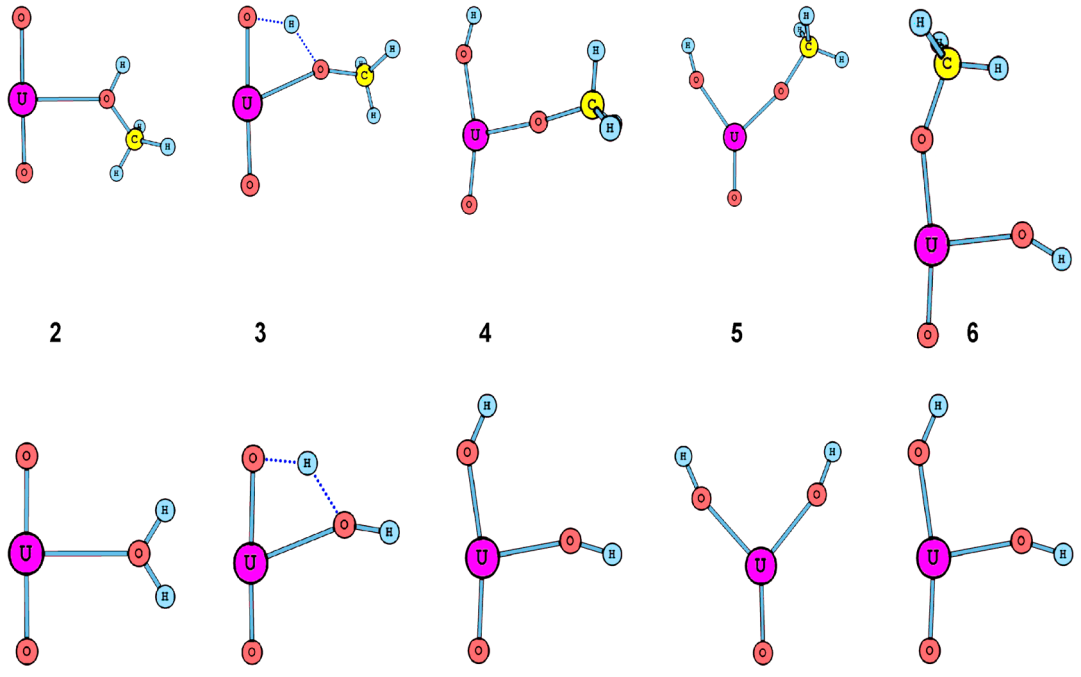

Figure 3. Structures of the species found in the potential energy profiles for oxo-exchange between UO_2^+ and methanol (top) or water (bottom). The structures are essentially the same for those for the reactions of NpO_2^+, PuO_2^+, and UO_2^{2+}. Structure **1** in the PEPs corresponds to separated UO_2^+ and CH_3OH or H_2O. The structural parameters for **2**, **3**, and **5** are in Supporting Information.

dx.doi.org/10.1021/ic402824k | Inorg. Chem. 2014, 53, 2163−2170

Table 5. Transition State Barriers Heights (3) of the 2−4 Reaction[a]

	water	methanol	ethanol	*i*-propanol	*t*-butanol
UO_2^+	143.7 (4.2)	129.9 (−17.5)	133.6 (−23.9)	138.3 (−27.8)	132.5 (−32.5)
NpO_2^+	147.4 (7.8)	147.2 (−12.4)	162.4 (−18.3)	164.1 (−23.2)	160.6 (−26.0)
PuO_2^+	177.2 (37.4)	173.7 (15.9)	181.5 (13.4)	180.8 (5.7)	176.6 (2.7)
UO_2^{2+}	227.9 (−51.9)	205.4 (−138.5)			

[a]The energies (kJ/mol) of **3** relative to the reactant asymptote, $AnO_2^{2+/+}$ + ROH, where R = H, CH_3, CH_3CH_2, $(CH_3)_2CH$, and $(CH_3)_3C$, are given in parentheses.

or methanol to create a hydroxyl O−H bond. The comparative energetics of the **2**−**3**−**4** reactions should reflect the ease with which the O_{yl} can be functionalized by hydrogen atoms from water or methanol. The ease of H-atom transfer is given by the bond dissociation energies: D[HO−H] = 499 kJ/mol and D[CH_3O−H] = 436 kJ/mol.[61] These energies suggest that more facile transfer of an H-atom from methanol versus water should result in an energetically more favorable **2**−**4** transformation for the former, as indicated by both the computed PEPs and the measured reaction kinetics. The greater association energies **1**−**2** of actinyl ions with methanol versus water lower the energies of the entire PEPs for methanol, further contributing to a lowering of the height of transition state **3** relative to the reactant energies.

Uranyl(V), Neptunyl(V), and Plutonyl(V). For NpO_2^+ and PuO_2^+, the PEPs and the structures of **1**−**6** are similar to those for UO_2^+ shown in Figures 2 and 3. For the oxo-exchange reactions of NpO_2^+ with water, and of PuO_2^+ with both water and methanol, the computed transition state **3** lies above the reactant energies (Table 5) such that it is predicted that the reactions should not occur; these reactions are not observed within the detection limit of $k/k_{COL} < 0.00002$. However, the transition state **3** for the NpO_2^+/methanol oxo-exchange reaction lies 12.4 kJ/mol below the reactant energies such that it is predicted that this reaction should occur; however, it was not observed to within the detection limit. This last example reveals that computed static PEPs cannot necessarily accurately predict all the details of dynamic processes such as oxo-exchange. It is feasible that the computed energy of transition state **3** for NpO_2^+/methanol could be in error, and/or that dynamic factors not considered in these computations preclude the reaction from occurring to within the detection limit. An implication of the apparent failure of the computed PEP to predict the nonobservation of the NpO_2^+/methanol oxo-exchange reaction is that the primary utility of static PEPs is for comparisons of general trends in reactivities, not for quantitative predictions of dynamic reaction rates. From the barrier heights **3** of the PEPs, it is predicted that NpO_2^+ should generally be less susceptible than UO_2^+ toward oxo-exchange, in accord with the experimental results.

Monopositive Uranyl versus Dipositive Uranyl. In the case of UO_2^{2+}, the oxo-exchange PEPs and structures of **1**−**6** are similar to those for UO_2^+. However, as is apparent from the PEPs shown in Figure 4 for the reactions of UO_2^{2+} with water and methanol, the energies of the intermediates **2** and **4** and the transition states **3** are very different from those for UO_2^+ (Figure 2). For both water and methanol, the transition state barrier heights for the **2**−**4** reaction are substantially greater for UO_2^{2+} (228 and 205 kJ/mol, Table 5) than for UO_2^+ (144 and 130 kJ/mol). The greater reactivity of the UO_2^{2+} is attributed to the much more favorable initial association energy of dipositive versus monopositive uranyl, by 140 kJ/mol with water and by 197 kJ/mol with methanol, to produce intermediate **2**. Due to

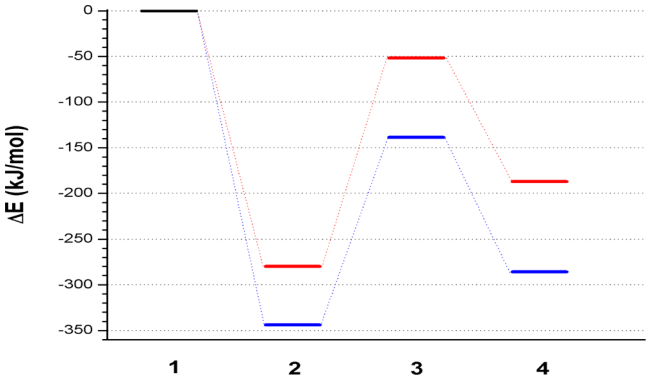

Figure 4. Section of the potential energy profiles for the oxo-exchange reactions of UO_2^{2+} with water (red) and methanol (blue). The energies are relative to the reactant asymptotes. The energies for **1**−**2** and **2**−**4** are in Tables 3 and 4, respectively. The transition state barrier heights (**3**) of the **2**−**4** reactions, as well as the energy of **3** relative to the reactant asymptote, are in Table 5. The structures of the species are essentially the same as for the UO_2^+ reactions, shown in Figure 3.

the greater association energies for the dipositive ions, the entire PEPs are shifted down. As a result, for UO_2^{2+} the transition states **3** lie well below the reactant energies, by 52 kJ/mol for water and by 139 kJ/mol for methanol, this despite that the **2**−**3** barriers are larger than for UO_2^+ (Figure 4). It was previously predicted that oxo-exchange with water should be more efficient for UO_2^{2+} than UO_2^+ in the gas phase,[27] which has now been experimentally confirmed.

The PEPs in Figures 2 and 4 can be used to predict relative oxo-exchange rates of UO_2^+ and UO_2^{2+} with water and methanol in solution under conditions where the mechanism involves the species shown in Figure 2, i.e., under acidic conditions. Perturbations to the energetics will be introduced by interactions with solvent species, but the general character of the PEPs should be similar in gas phase and in solution. A significant difference is that the initial state in the gas phase reaction corresponds to the separated ion and neutral ligand, whereas the initial state in solution corresponds to an ion that is already fully solvated. Accordingly, the energy provided by the association reaction **1**−**2** is absent in solution; the solution PEPs can be approximated as starting at the association intermediate **2** such that the **2**−**3** energy barrier heights provide a prediction of comparative oxo-exchange rates in solution. From the values in Table 5 it is apparent that the **2**−**3** barrier heights are substantially greater for UO_2^{2+} than UO_2^+, by 84 kJ/mol with water and by 76 kJ/mol with methanol. Whereas gas-phase exchange is predicted and observed to proceed more efficiently for UO_2^{2+} with both water and methanol, the prediction is that solution exchange should be more efficient for UO_2^+ with both, as has been demonstrated in the case of

dx.doi.org/10.1021/ic402824k | Inorg. Chem. 2014, 53, 2163−2170

water;[8] uranyl/methanol exchange in solution has not yet been reported.

Comparative PEPs for Water, Methanol, and Larger Alcohols. Reaction energetics were computed for the reactions of AnO_2^+ (An = U, Np, Pu) and UO_2^{2+} with ethanol (EtOH), *i*-propanol (*i*-PrOH), and *t*-butanol (*t*-BuOH); the results are included in Tables 3−5. The **1**−**2** association reactions are more exothermic for methanol versus water, and become increasingly exothermic as the size of the alcohol increases (Table 3). The following gas-phase basicities of the neutral O-atom donors (kJ/mol), derived from proton affinities, provide an indication of the ability to bind to a positively charged metal center:[62]

$$H_2O/660 < MeOH/724 < EtOH/746 < i\text{-}PrOH/763 < t\text{-}BuOH/772$$

The association energies between the actinyl cations and the O-atom donors generally correlate with these gas-phase basicities. The computed association energies for *i*-PrOH and *t*-BuOH for a given AnO_2^+ are nearly the same; although the basicity of *t*-BuOH is greater than that of *i*-PrOH, the difference is only 9 kJ/mol. The transition state **3** barrier heights relative to the reactant energies decrease from water to MeOH and continue to decrease as the size of the alcohol increases, an effect that can be largely attributed to the increasing **1**−**2** association energies and resulting lowering of the entire PEPs.

Possible Role of Covalency in Actinyl Exchange. It was previously postulated that the more facile oxo-exchange with water of UO_2^+ versus NpO_2^+ and PuO_2^+ could be attributed to increasing covalency across the actinyl series.[27] The rationale was that formation of intermediate **4** requires disruption of the An═O bond to produce two ionic An−OH bonds. The barrier to this process should not necessarily reflect the intrinsic An═O bond energy, but rather the covalent component of the bonding that is disrupted, which evidently increases from UO_2^+ to PuO_2^+. The same effect has now been revealed in the experimental results and the PEPs for exchange of the actinyl(V) ions with methanol. We here provide bonding analyses to evaluate covalency in the actinyls.

The axial An-O_{yl} bonds in the $AnO_2(CH_3OH)^+$ complexes **2** are calculated to be about 1.767, 1.757, and 1.739 Å long for the uranyl, neptunyl, and plutonyl species, respectively. A similar contraction is obtained for the bare AnO_2^+ species (Table 6), as well as for the $AnO_2(H_2O)^+$ complexes. These values are consistent with the actinide contraction and do not necessarily reveal any variation in bonding across the series.[63]

Table 6. Calculated Lengths and Strengths (kJ/mol) of the An-O_{yl} Bonds[a]

	An-O_{yl} (Å)	Pauli repulsion interaction energy	electrostatic interaction energy	orbital interaction energy	total
UO_2^+	1.760	6714	−16770	−5451	−15507
NpO_2^+	1.741	6827	−16977	−5930	−16080
PuO_2^+	1.723	6932	−17165	−6307	−16540
UO_2^{2+}	1.701	7645	−20279	−7473	−20107
NpO_2^{2+}	1.697	7814	−20302	−8216	−20704
PuO_2^{2+}	1.683	7858	−20467	−8843	−21452

[a]The latter is defined as the $(O^{2-})_2$-An^{5+} and $(O^{2-})_2$-An^{6+} binding energies for the pentavalent and hexavalent species, respectively.

To evaluate the degree of covalency in the actinyls, we analyzed the binding energies of the $(O^{2-})_2$ to the An^{5+} and An^{6+} centers in AnO_2^+ and AnO_2^{2+}, with the results presented in Table 6. The total binding energies increase from uranyl to neptunyl to plutonyl for both the +1 and +2 actinyls. It should be remarked that these intrinsic binding energies do not correspond to measured bond dissociation energies to neutral O and $An^{+/2+}$, which contrastingly *decrease* from $UO_2^{+/2+}$ to $NpO_2^{+/2+}$ to $PuO_2^{+/2+}$.[2] The computed orbital interaction energies of the $AnO_2^{+/2+}$ as $(O^{2-})_2$-An^{5+} and $(O^{2-})_2$-An^{6+} provide an indication of the transfer of electron density, which is evidently greatest for plutonyl in both the actinyl(V) and actinyl(VI) series. Experimental bond energies for the actinyls correspond to the reactions: $An^{+/2+} + 2O \rightarrow AnO_2^{+/2+}$. Bond energy decomposition analysis[57−59] with An^{2+} and atomic oxygen fragments indicate orbital interaction energies of −4386, −4172, and −4903 kJ/mol for UO_2^{2+}, NpO_2^{2+}, and PuO_2^{2+}, respectively (Table S2). For the analogous pentavalent AnO_2^+, the orbital interaction energies when An^+ is the considered fragment are calculated as −5003, −4299, and −4228 kJ/mol, respectively. This alternative analysis to that presented in Table 6 suggests a *decrease* in covalency from UO_2^+ to PuO_2^+. It is apparent that these binding energy decompositions do not provide a clear indication of the extent of covalency.

The calculated Mulliken charges for the AnO_2^+ and AnO_2^{2+} complexes (Table 7) may suggest increasing covalency across the actinyl series because the electron density at the axial oxygen atoms is largest for uranyl and smallest for plutonyl. The implication from this analysis is that the plutonyl complexes have the highest overlap (most covalent) of the 5f/6d orbitals with the atomic 2p orbitals of the axial oxygen atoms. In qualitative accord with this interpretation is the trend in the calculated Mayer bond orders[64,65] of the axial bonds: Pu−O_{yl} > Np−O_{yl} > U−O_{yl} (Table 8). However, the Mayer bond orders increase by only 0.03 from $UO_2^{+/2+}$ to $PuO_2^{+/2+}$, which is too small a change to clearly indicate an increase in covalency.

Analysis of the An-O bonds in the actinyl moieties with the atoms in molecules (AIM) approach[66,67] shows little difference in the Laplacian of the electron density obtained at the bond critical points between the actinide and oxygen atoms of the AnO_2^{2+} and AnO_2^+ species (Figure S2). However, Prodan et al. have proposed that covalency increases across the series of actinide dioxides due to a 5f-O2p orbital energy degeneracy, not due to the conventional concept of covalency as an increase in charge density between atoms.[31] Kaltsoyannis has discussed this nontraditional concept of covalency in the particular context of organoactinide complexes, with caution that "care must be taken when using quantum chemistry to assess metal−ligand covalency in this part of the periodic table."[35] We concur with this assessment. In summary, the computed orbital interaction energies seem to provide conflicting indications of covalency, the Mulliken charges may indicate an increase in covalency from uranyl to plutonyl, and the small changes in the Mayer bond orders are essentially inconclusive regarding a change in covalency from uranyl to plutonyl. However, the experimental results and computed PEPs are consistent with such an increase in covalency, as has been discussed previously.[27] The increase in the **2**−**3**−**4** energy in the PEPs from uranyl to plutonyl is clearly manifested in the experimental results. Conversion of **2** to **4** disrupts the An═O bond to produce two less directional and more ionic An-OR

dx.doi.org/10.1021/ic402824k | Inorg. Chem. 2014, 53, 2163−2170

Table 7. Calculated Mulliken Atomic Charges on the Actinide Atoms of AnO_2^+, $AnO_2(H_2O)^+$, and $AnO_2(CH_3OH)^+$[a]

	pentavalent			hexavalent	
	AnO_2^+	$AnO_2(H_2O)^+$	$AnO_2(CH_3OH)^+$	AnO_2^{2+}	$AnO_2(CH_3OH)^{2+}$
U	2.10 (−0.55)	2.03 (−0.58)	2.03 (−0.60)	2.72 (−0.36)	2.55 (−0.44)
Np	2.01 (−0.51)	1.96 (−0.55)	1.96 (−0.56)	2.60 (−0.30)	[b]
Pu	1.97 (−0.48)	1.94 (−0.53)	1.93 (−0.54)	2.53 (−0.26)	2.36 (−0.37)

[a]The charges on the axial oxygen atoms are given in parentheses. [b]Value not computed.

Table 8. Calculated Mayer Bond Orders of the An-O_{yl} Bonds of the $AnO_2^{2+/+}$, $AnO_2(H_2O)^+$, and $AnO_2(CH_3OH)^{2+/+}$ Species

	pentavalent			hexavalent	
	AnO_2^+	$AnO_2(H_2O)^+$	$AnO_2(CH_3OH)^+$	AnO_2^{2+}	$AnO_2(CH_3OH)^{2+}$
U	2.15	2.11	2.10	2.29	2.21
Np	2.18	2.14	2.12	2.31	2.22
Pu	2.18	2.15	2.13	2.32	2.23

bonds (R = H or CH_3). Despite that $D[OU\text{-}O]^+ = 741 \pm 14$ kJ/mol is larger than $D[OPu\text{-}O]^+ = 509 \pm 38$ kJ/mol,[2] the **2**−**4** barrier for UO_2^+ (144 kJ/mol) is lower than for PuO_2^+ (177 kJ/mol)—greater resistance of the weaker $[OPu\text{-}O]^+$ toward disruption is consistent with greater directionality, in this case linearity, and thus covalency. The present results do not establish the postulated increase in covalency from uranyl to plutonyl, but are at least consistent with it.

CONCLUSIONS

It had previously been demonstrated that oxo-exchange reactions of actinyls in the gas phase could illuminate mechanisms in solution, specifically under acidic conditions where hydrolysis is suppressed and the dominant species are AnO_2^+ and/or AnO_2^{2+}.[27] The comparative gas-phase oxo-exchange rates previously reported for UO_2^+, NpO_2^+, and PuO_2^+ with H_2O have now been quantified with the pseudo-first-order rate constant for UO_2^+, and limits for NpO_2^+ and PuO_2^+. It was previously predicted that gas-phase exchange with UO_2^{2+} should be faster than with UO_2^+. In the present work it was demonstrated that exchange with UO_2^{2+} is at least 100 times faster than with UO_2^+, validating the prediction.

Oxo-exchange of UO_2^+, NpO_2^+, PuO_2^+, and UO_2^{2+} with methanol was studied in the present work. The PEPs for exchange with water and methanol were computed, revealing similar mechanisms. The largest barrier on the reaction pathways is to the first intermediate bis-hydroxy or hydroxy-methoxy species produced by transfer of an H-atom from a coordinated water or methanol molecule to an actinyl oxo-group. These barrier heights are lower for methanol versus water, an effect attributed primarily to cleavage of the weaker CH_3O−H bond as compared with the HO-H bond. The measured rate constants reveal faster exchange with methanol versus water, in accord with the computed PEPs, and providing validation of the DFT methodology.

Gas-phase results can be used to predict comparative exchange rates in solution. A crucial difference between gas and solution is that the association energies between actinyl ions available to enable the reactions in gas phase are absent in solution. Gas-phase kinetics of bimolecular reactions are related to the energy of the highest barrier relative to the energies of the reactants: for barriers significantly above the reactant energies, the reaction should not proceed; for barriers significantly below the reactant energies, the reaction should proceed; for reactions with barriers close to the reactant energies (e.g., within ca. 10 kJ/mol), predictions are less reliable. In solution phase, it is the absolute height of the barrier that predicts relative kinetics. Thus it is predicted that for water, gas-phase exchange should be more efficient with UO_2^+ than with UO_2^{2+}, whereas the opposite relative rates are predicted in solution; these comparative kinetics have now been demonstrated. It is predicted that UO_2^+ and UO_2^{2+} should exchange more efficiently with methanol than water in both gas and solution phases; this has been demonstrated in gas phase; actinyl/methanol exchange in solution has yet to be studied.

The experimental result and DFT prediction that oxo-exchange should be decreasingly efficient from UO_2^+ to PuO_2^+ can be taken to suggest greater covalency of the actinyl bonds upon proceeding across the actinyl series. Although analysis of actinyl binding energies was inconclusive in evaluating covalency, the computed Mulliken atomic charges are in accord with a covalency increase across the actinyl series. Further analysis is needed to clarify this covalency issue.[35]

ASSOCIATED CONTENT

Supporting Information

Experimental Details; Lengths and strengths of the equatorial U−O bonds in $[UO_2(H_2O)]^+$ and $[UO_2(CH_3OH)]^+$; Strengths of the An-O_{yl} bonds, defined as the $(O)_2$-An^+ and $(O)_2$-An^{2+} binding energies; Bond Distances for **2**, **3**, and **5** in Figure 3; Calculated Laplacian of the electron density at the An-O bond critical points using AIM; Cartesian coordinates of species found on the PEPs. This material is available free of charge via the Internet at http://pubs.acs.org.

AUTHOR INFORMATION

Corresponding Authors

*E-mail: schrecke@cc.umanitoba.ca.

*E-mail: jkgibson@lbl.gov.

Author Contributions

△A. F. Lucena performed most of the experimental work. S. O. Odoh performed most of the computational work.

Notes

The authors declare no competing financial interest.

ACKNOWLEDGMENTS

This work was supported by Fundação para a Ciência e a Tecnologia/Portugal (PhD grant SFRH/BD/70475/2010 to A.F.L.), by the Natural Sciences and Engineering Research Council of Canada (NSERC, G.S.), and by the U.S.

Department of Energy, Office of Science, Office of Basic Energy Sciences, Division of Chemical Sciences, Geosciences and Biosciences, Heavy Element Chemistry Program at LBNL under Contract Number DE-AC02-05CH11231 (J.K.G.).

REFERENCES

(1) Morss, L. R.; Edelstein, N. M.; Fuger, J. *The Chemistry of the Actinide and Transactinide Elements*; Springer: Dordrecht, 2006.
(2) Marçalo, J.; Gibson, J. K. *J. Phys. Chem. A* **2009**, *113*, 12599.
(3) Fortier, S.; Hayton, T. W. *Coord. Chem. Rev.* **2010**, *254*, 197.
(4) Baker, R. J. *Chem.—Eur. J.* **2012**, *18*, 16258.
(5) Burns, C. J.; Sattelberger, A. P. *Inorg. Chem.* **1988**, *27*, 3692.
(6) Arnold, P. L.; Pecharman, A. F.; Hollis, E.; Yahia, A.; Maron, L.; Parsons, S.; Love, J. B. *Nat. Chem.* **2010**, *2*, 1056.
(7) Gordon, G.; Taube, H. *J. Inorg. Nucl. Chem.* **1961**, *19*, 189.
(8) Gordon, G.; Taube, H. *J. Inorg. Nucl. Chem.* **1961**, *16*, 272.
(9) Rabideau, S. W.; Hecht, H. G. *J. Chem. Phys.* **1967**, *47*, 544.
(10) Jurisson, S. S.; Murmann, R. K. *Inorg. Chem.* **1999**, *38*, 3919.
(11) Rabideau, S. W. *J. Phys. Chem.* **1967**, *71*, 2747.
(12) Clark, D. L.; Conradson, S. D.; Donohoe, R. J.; Keogh, D. W.; Morris, D. E.; Palmer, P. D.; Rogers, R. D.; Tait, C. D. *Inorg. Chem.* **1999**, *38*, 1456.
(13) Clark, D. L.; Conradson, S. D.; Donohoe, R. J.; Gordon, P. L.; Keogh, D. W.; Palmer, P. D.; Scott, B. L.; Tait, C. D. *Inorg. Chem.* **2013**, *52*, 3547.
(14) Rabideau, S. W. *J. Phys. Chem.* **1963**, *67*, 2655.
(15) Masters, B. J.; Rabideau, S. W. *Inorg. Chem.* **1963**, *2*, 1.
(16) Tsushima, S. *Inorg. Chem.* **2012**, *51*, 1434.
(17) Wang, D. Q.; van Gunsteren, W. F.; Chai, Z. F. *Chem. Soc. Rev.* **2012**, *41*, 5836.
(18) Bühl, M.; Wipff, G. *ChemPhysChem* **2011**, *12*, 3095.
(19) Bühl, M.; Schreckenbach, G. *Inorg. Chem.* **2010**, *49*, 3821.
(20) Szabo, Z.; Grenthe, I. *Inorg. Chem.* **2010**, *49*, 4928.
(21) Schreckenbach, G.; Shamov, G. A. *Acc. Chem. Res.* **2010**, *43*, 19.
(22) Real, F.; Vallet, V.; Wahlgren, U.; Grenthe, I. *J. Am. Chem. Soc.* **2008**, *130*, 11742.
(23) Shamov, G. A.; Schreckenbach, G. *J. Am. Chem. Soc.* **2008**, *130*, 13735.
(24) Szabo, Z.; Grenthe, I. *Inorg. Chem.* **2007**, *46*, 9372.
(25) Wahlin, P.; Danilo, C.; Vallet, V.; Real, F.; Flament, J. P.; Wahlgren, U. *J. Chem. Theory Comput.* **2008**, *4*, 569.
(26) Schreckenbach, G.; Hay, P. J.; Martin, R. L. *Inorg. Chem.* **1998**, *37*, 4442.
(27) Rios, D.; Michelini, M. D.; Lucena, A. F.; Marçalo, J.; Gibson, J. K. *J. Am. Chem. Soc.* **2012**, *134*, 15488.
(28) Glueckauf, E.; Mckay, H. A. C. *Nature* **1950**, *166*, 605.
(29) Denning, R. G. *J. Phys. Chem. A* **2007**, *111*, 4125.
(30) Neidig, M. L.; Clark, D. L.; Martin, R. L. *Coord. Chem. Rev.* **2013**, *257*, 394.
(31) Prodan, I. D.; Scuseria, G. E.; Martin, R. L. *Phys. Rev. B* **2007**, *76*.
(32) Ingram, K. I. M.; Tassell, M. J.; Gaunt, A. J.; Kaltsoyannis, N. *Inorg. Chem.* **2008**, *47*, 7824.
(33) Tassell, M. J.; Kaltsoyannis, N. *Dalton Trans.* **2010**, *39*, 6719.
(34) Kirker, I.; Kaltsoyannis, N. *Dalton Trans.* **2011**, *40*, 124.
(35) Kaltsoyannis, N. *Inorg. Chem.* **2013**, *52*, 3407.
(36) Gibson, J. K.; Haire, R. G.; Santos, M.; Marçalo, J.; Pires de Matos, A. *J. Phys. Chem. A* **2005**, *109*, 2768.
(37) Santos, M.; Marçalo, J.; Pires de Matos, A.; Gibson, J. K.; Haire, R. G. *J. Phys. Chem. A* **2002**, *106*, 7190.
(38) Marçalo, J.; Santos, M.; Pires de Matos, A.; Gibson, J. K. *Inorg. Chem.* **2009**, *48*, 5055.
(39) Su, T.; Chesnavich, W. J. *J. Chem. Phys.* **1982**, *76*, 5183.
(40) Valiev, M.; Bylaska, E. J.; Govind, N.; Kowalski, K.; Straatsma, T. P.; Van Dam, H. J. J.; Wang, D.; Nieplocha, J.; Apra, E.; Windus, T. L.; de Jong, W. *Comput. Phys. Commun.* **2010**, *181*, 1477.
(41) te Velde, G.; Bickelhaupt, F. M.; van Gisbergen, S. J. A.; Fonseca Guerra, C.; Baerends, E. J.; Snijders, J. G.; Ziegler, T. *J. Comput. Chem.* **2001**, *22*, 931.
(42) Bergner, A.; Dolg, M.; Küchle, W.; Stoll, H.; Preuss, H. *Mol. Phys.* **1993**, *80*, 1431.
(43) Küchle, W.; Dolg, M.; Stoll, H.; Preuss, H. *Mol. Phys.* **1991**, *74*, 1245.
(44) Küchle, W.; Dolg, M.; Stoll, H.; Preuss, H. *J. Chem. Phys.* **1994**, *100*, 7535.
(45) Godbout, N.; Salahub, D. R.; Andzelm, J.; Wimmer, E. *Can. J. Chem.-Rev. Can. Chim.* **1992**, *70*, 560.
(46) Becke, A. D. *J. Chem. Phys.* **1993**, *98*, 5648.
(47) Stephens, P. J.; Devlin, F. J.; Chabalowski, C. F.; Frisch, M. J. *J. Phys. Chem.* **1994**, *98*, 11623.
(48) de Jong, W. A.; Apra, E.; Windus, T. L.; Nichols, J. A.; Harrison, R. J.; Gutowski, K. E.; Dixon, D. A. *J. Phys. Chem. A* **2005**, *109*, 11568.
(49) de Jong, W. A.; Harrison, R. J.; Nichols, J. A.; Dixon, D. A. *Theor. Chem. Acc.* **2001**, *107*, 22.
(50) Odoh, S. O.; Schreckenbach, G. *J. Phys. Chem. A* **2010**, *114*, 1957.
(51) Odoh, S. O.; Schreckenbach, G. *J. Phys. Chem. A* **2011**, *115*, 14110.
(52) Odoh, S. O.; Walker, S. M.; Meier, M.; Stetefeld, J.; Schreckenbach, G. *Inorg. Chem.* **2011**, *50*, 3141.
(53) Shamov, G. A.; Schreckenbach, G. *J. Phys. Chem. A* **2005**, *109*, 10961.
(54) Shamov, G. A.; Schreckenbach, G.; Vo, T. N. *Chem.—Eur. J.* **2007**, *13*, 4932.
(55) van Lenthe, E.; Baerends, E. J.; Snijders, J. G. *J. Chem. Phys.* **1993**, *99*, 4597.
(56) van Lenthe, E.; Ehlers, A.; Baerends, E. J. *J. Chem. Phys.* **1999**, *110*, 8943.
(57) Mitoraj, M. P.; Michalak, A.; Ziegler, T. *J. Chem. Theory Comput.* **2009**, *5*, 962.
(58) Mitoraj, M. P.; Michalak, A.; Ziegler, T. *Organometallics* **2009**, *28*, 3727.
(59) Ziegler, T.; Rauk, A. *Theor. Chim. Acta* **1977**, *46*, 1.
(60) Rutkowski, P. X.; Michelini, M. C.; Bray, T. H.; Russo, N.; Marçalo, J.; Gibson, J. K. *Theor. Chem. Acc.* **2011**, *129*, 575.
(61) Lias, S. G.; Bartmess, J. E.; Liebmann, J. F.; Holmes, J. L.; Levin, R. D.; Mallard, W. G. *Gas-Phase Ion and Neutral Thermochemistry*; American Institute of Physics: New York, 1988.
(62) Hunter, E. P.; Lias, S. G. In *NIST Chemistry WebBook, NIST Standard Reference Database Number 69*; Linstron, P. J., Mallard, W. G., Eds.; National Institute of Standards and Technology: Gaithersburg, MD.
(63) Wang, S. A.; Villa, E. M.; Diwu, J. A.; Alekseev, E. V.; Depmeier, W.; Albrecht-Schmitt, T. E. *Inorg. Chem.* **2011**, *50*, 2527.
(64) Mayer, I. *Int. J. Quantum Chem.* **1984**, *26*, 151.
(65) Mayer, I. *Int. J. Quantum Chem.* **1986**, *29*, 477.
(66) Rodriguez, J. I.; Bader, R. F. W.; Ayers, P. W.; Michel, C.; Gotz, A. W.; Bo, C. *Chem. Phys. Lett.* **2009**, *472*, 149.
(67) Rodriguez, J. I.; Koster, A. M.; Ayers, P. W.; Santos-Valle, A.; Vela, A.; Merino, G. *J. Comput. Chem.* **2009**, *30*, 1082.